Characterization and Phase Transformation of Spherical YSZ Powders Fabricated Via air Plasma Spray Method

M.R. Dadfar [a], M.R. Rahimipour [a,*], M.R. Vaezi [a], A. Gholamzadeh [b]

[a]*Department of Ceramic, Materials and Energy Research Center, Karaj, Iran*
[b]*Department of Materials Science and Engineering, Sharif University of Technology, Tehran, Iran*

ABSTRACT

Air plasma spray (APS) process is used to produce high density and flowability spherical powders. Phase transformation that occurred in this process isn't well known. In this paper, the YSZ powders have been sprayed in water to investigate the morphology changes and phase transformations via air plasma spray (APS) method. Phase analysis of powders was examined by XRD and the crystallite size and lattice strain of YSZ calculated by the Williamson-Hall method. Morphology and particle size measurement observed by scanning electron microscope. Therefore, results showed the good spherical YSZ powders morphology and amount of tetragonal phase at this process changes from 33 to 47 wt%. that phase transformations were in order to improve the properties of the fabricated powders. Decreasing the crystalline size is due to tetragonal crystallite formation as first monoclinic crystallite (from 91 nm to 70 nm).

1. INTRODUCTION

In many applications such as coatings, electronics, catalysis and etc, powders are used in the manufacturing and development of products, parts, tools and instruments [1]. Powder quality can affect coating performance through one or more of the following effects: the powder feedstock morphology and particle size distribution, the transport properties of the powders and the injection technique used [2, 3].

Spray techniques are suitable for manufacturing a wide range of powders with controlled properties, simply. One of these techniques is spray drying. During the spray drying process, the rapid heat and mass transfer occurs during drying process results in dried granules with a wide variety of shapes [4 , 5].

Another spray technique is Atmospheric plasma spray (APS). In recent years, plasma process was used to produce high density and flowability spherical powders [2, 6]. High temperature plasma flame produces surface melting metal and ceramic powders which then they cooled quickly on the surface substrate. Plasma spraying is a cost-effective technology to manufacture MCrAlY (M=Ni, Co or Ni/Co) and thermal barrier coatings (TBC) coatings. The powder particles are injected into the plasma jet by a carrier gas, and melted and accelerated toward the substrate, where they impact at high speed and quench, thus producing the build-up of a coating with unique microstructure. Control factors having direct correlations with the processing parameters. These control factors are the velocity and temperature of the feedstock powder particles during their flight [7].

The physical, chemical and morphological characteristics of these powders play a predominant role in the specifications of the coating. Powders with adequate granule morphology lead to good flowability and powders enter the plasma jet without problems. The spheroidized powders are formed by rapid solidification of the individual droplets. The high cooling rate also tends to form different phases at ambient temperatures than for sintered ceramic of the same composition. The resulting powders have good flowability with low porosity that is suitable for plasma spray process [8, 9]. For producing the plasma sprayable powder, the spherical morphology has these advantages: improvement of powder flowability, enhancement of powder packing density, elimination of particle internal cavities and fractures, and alteration of particle surface morphology [10].

TBCs are potential tools for coating metallic substrate parts and increasing the efficiency of thermal engines [11]. These coatings consist of a metallic bond coat which is typically MCrAlY and a ceramic topcoat which

Corresponding Author's Email: m-rahimipour @merc.ac.ir (M.R. Rahimipour)

is typically Yttria Stabilized Zirconia (YSZ). The porous ceramic top coat, which is typically 6 to 8 wt.% Y_2O_3-stabilized ZrO_2 (YSZ), protects the underlying air-cooled engine component by significantly reducing its operating temperature [12, 13], while the adherent bond coat provides high temperature oxidation protection of the underlying super alloy components in the most hot sections of gas turbines, as well as good conjunction with an upper ceramic TBC [14-19].

By using and directing a stream of high-velocity APS to spray the powders into distilled water, fine particle sized and granule powders can be prepared. As mentioned, the surface molten 8YSZ powder also will change into a sphere shape.

Therefore, this study is aimed to investigate the influence of sprayed powder in water on the morphologies and phase transformations of YSZ powders.

2. EXPERIMENTAL

The composition and commercial characterization of YSZ used in this work are listed in Table 1.

TABLE 1. Composition and commercial characterization of YSZ

	Particle size (µm)	PAC number
Zirconia–Yttria 8% stabilized powder	+15-106	2008P

Powders were sprayed in water using the atmospheric plasma spraying system equipped with METCO 3M type plasma gun. The primary plasma gas was Argon and Hydrogen, added as the secondary gas. The processing parameters of powder spraying are reported in Table 2.

TABLE 2. Processing parameters of powders spraying

Voltage (V)	Current (A)	Primary argon flow rate (SLPM)	Secondary Hydrogen flow rate (SLPM)	Powder feed rate (g/min)	Carrier gas flow rate (SLPM)
55	500	80	15	15-20	40

The morphology of the powders, before and after plasma spraying was examined using a S360 Cambridge scanning electron microscope (SEM). The X-ray diffraction (Philips Mode, PW 3710) measurements were carried out using Cu-Ka (λ=0.154 nm) at 40 kV and 30 mA for phase identification and structure analysis. The step width and scan speed of diffraction studied were 0.02° and 0.04°/s respectively. The crystallite size and strain of YSZ powders before and after spraying in water were evaluated from width of the XRD patterns peak through Williamson–Hall method [20]. In this method, crystalline size, D, is given by:

$$b \cos\theta = (0.9 \lambda/d) + 2 \eta \sin\theta \qquad (1)$$

Where b is the FWHM, θ the diffraction angle, λ the wavelength of the X-ray, and η is the effective strain. The crystalline size D can be obtained by extrapolating $\sin\theta$ to zero to eliminate the strain term. The crystallite size is calculated from full width at half maximum (FWHM) of the cubic phase peaks (111) (200) (220) and (311). The Bragg peak breadth is a combination of both instrument and sample dependent effects. To remove these aberrations, it is needed to assemble a diffraction pattern from the line broadening of a standard material such as silicon to determine the instrumental broadening.

3. RESULT AND DISCUSSION

As is known, crystallite size of the nanocrystalline materials strongly effect on their mechanical and physical properties [21]. There are a large number of grain boundaries in small crystallite size, which

preparing more atoms ready to react. It is well proven that the reactivity of materials can be improved with the lattice strain increase and a crystallite size reduction [22]. So the determination of the crystallite size and lattice strain by X-ray profile analysis is great importance. These values could be extracted from the peak width analysis. Bragg peak is affected by crystallite size and lattice strain which increase the peak width and intensity shifting the 2θ peak position accordingly.

Fig. 1 (a) and (b) shows the XRD patterns of YSZ powders before and after spraying in water, respectively. All the diffraction peaks can be assigned to three phases (cubic, tetragonal and monoclinic).

Depending on different θ positions the separation of size and strain broadening analysis is done using Williamson-Hall and the size-strain plot method.

The diffraction peaks of the XRD pattern before and after spraying in water are used to construct a linear plot of b $\cos\theta$ against 4 $\sin\theta$ (Fig. 2 (a) and (b)). Then, the crystallite size is obtained from the intercept the strain from the slope of the fit.

From the results shows in Fig. 3 (a) and (b), it was observed that the strain value and crystallite size decreased after spraying in water.

The decrease of microstrain results in the regression line slopes going down as presented in Williamson-Hall plots. As it is clear, heat induced to the powders release some stress and as a result strain value will be decreased. On the other hand, more stress will produce during the rapid water cooling. These are two mechanisms that occurred and were in competition together in the APS fabrication process. Depending on the amount of heat induced to the powders in APS

process, water temperature and distance of the gun to the water container, one of these mechanisms can be overcome. In this case, release stress results from heat induced overcame. The results were reasonable with the strain obtained from the XRD where large ε gives down to small one. Decreasing the crystalline size is due to tetragonal crystallite formation (nuclei and growth) and

new grains can't grow as well as first monoclinic crystallite (from 91 nm to 70 nm).

The crystal size and morphology depend upon the relative nucleation and growth rates of crystals from the melt. In most cases it seems that rapid nucleation occurs at the cooler surface of the powders at large under cooling and the crystals grow rapidly in the opposite direction to heat flow [23].
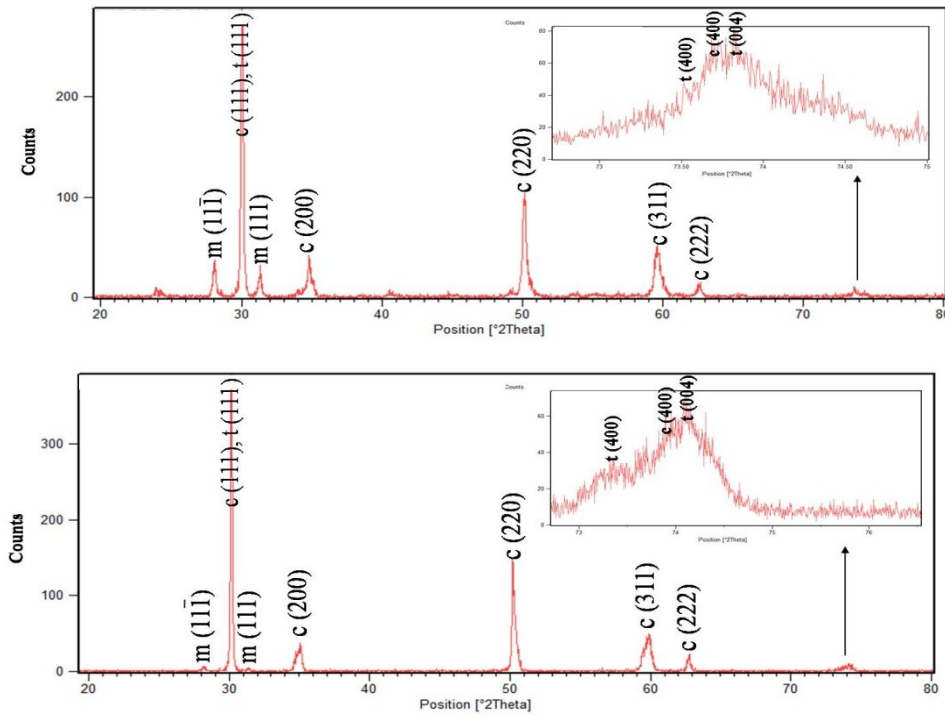

Figure 1. XRD pattern of YSZ (a) before spraying in water and (b) after spraying in water
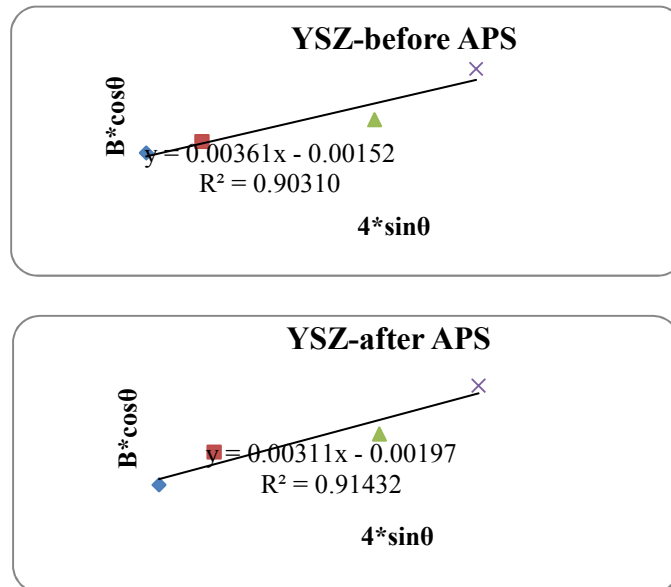

Figure 2. Williamson-Hall curve of YSZ (a) before spraying in water and (b) after spraying in water
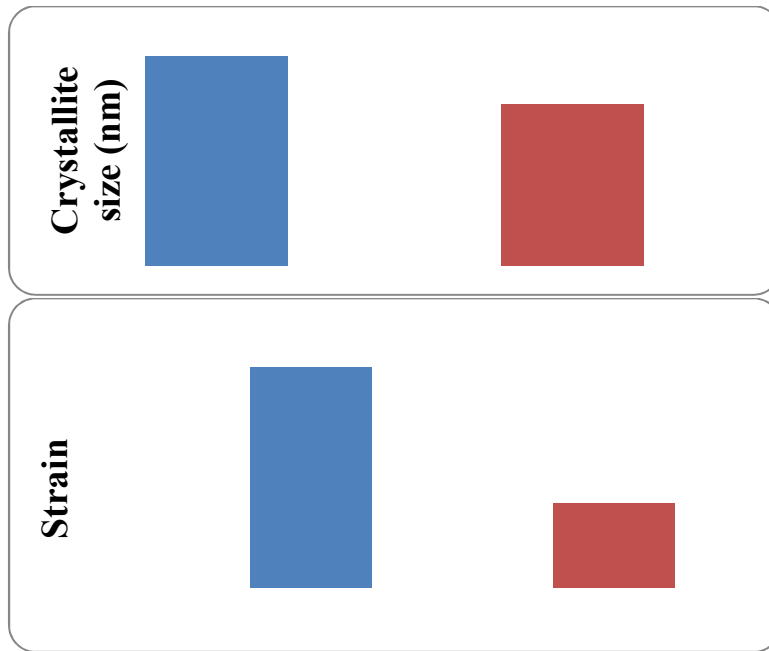
Figure 3. (a) Crystallite size and (b) Lattice strain of YSZ before and after spraying in water

The ZrO_2 based coatings prepared by plasma spraying are formed from any of the three phases: monoclinic, tetragonal and cubic phases. The presence of the cubic and tetragonal phases is confirmed by XRD by using (400) and (004) peaks. The amounts of monoclinic, tetragonal and cubic phases were calculated according to the following equations [24]:

$$C_m = \frac{0.82\{I_m(11\bar{1}) + I_m(111)\}}{0.82\{I_m(11\bar{1}) + I_m(111)\} + I_{t,c}(111)} \quad (2)$$

$$C_t = (1 - C_m)\frac{1.14\{I_t(400) + I_t(004)\}}{1.14\{I_t(400) + I_t(004)\} + I_c(400)} \quad (3)$$

$$C_c = 1 - (C_m + C_t) \quad (4)$$

Where I_m, I_t and I_c are the integrated intensity area of the monoclinic, tetragonal and cubic peaks, respectively.

C_m, C_t and C_c are the mole fractions of monoclinic, tetragonal and cubic phases, respectively.

There is, interest in the formation of metastable t-ZrO_2 phase in addition to the stable cubic phase, but recent studies on rapidly solidified ZrO_2-Y_2O_3 as stabilized Zirconia systems shows the formation of a nontransformable phase that called t' [25-27].

Table 3, gives the mole fractions C_m, C_t and C_c calculated this way. The YSZ powders before and after spraying in water were phased analyzed. It is well known that at 8 wt.% Y_2O_3 content (with reference to the ZrO_2-Y_2O_3 phase diagram in Fig. 4) after spraying in water the monoclinic phase transform to the tetragonal phase predominates, and cubic phase remained constant. After spraying, most of the powders became stabilized Zirconia.

There are different theories and hypotheses to explain metastability of the high-temperature phases (c- and t-ZrO_2) at ambient temperatures but the controlling mechanisms responsible are unknown clearly. Up to now, this monoclinic to tetragonal transformation has been explained as related to the size distribution of Zirconia grains, *i.e.* a narrow grain size distribution leads to a well-defined transformation zone (higher monoclinic), and a wide grain size distribution results in a more diffuse transformation zone (lower monoclinic) [28]. It can therefore be presumed that the average crystallite size existing in the Fig. 3 (a) is in good agreement with the phase analysis in Table 3. Many monoclinic crystallite with larger crystallite size transform to tetragonal crystallite.

It has also been suggested that some of the m- and c-ZrO_2 present in an as-sprayed ZrO_2-(8 wt.%)Y_2O_3 powder is a result of a diffusion transformation that may take place by reduction of the cooling rate during the plasma spraying process [29]. With reference to the ZrO_2-Y_2O_3 phase diagram at 8wt. % Y_2O_3 (Fig. 4), if diffusion occurred during the cooling of the plasma sprayed ZrO_2-Y_2O_3, the t-ZrO_2 would decompose into c-ZrO_2. The m-ZrO_2 observed in the as-sprayed ZrO_2-Y_2O_3 powder has also been attributed to the martensitic m-ZrO_2 transformation, which again occurred during the plasma spraying process. A displacive and diffusionless transformation process has been described for quenched ZrO_2-Y_2O_3, where diffusion has been limited by the fast cooling rate.

Fig. 5 shows the morphology of the YSZ before and after plasma spheroidizing process by spraying in water method. YSZ powder morphology was changed from an

irregular or semi-spherical shape to spherical shape after the APS process. The flowability of the non spherodized powders is passable (41 degree).
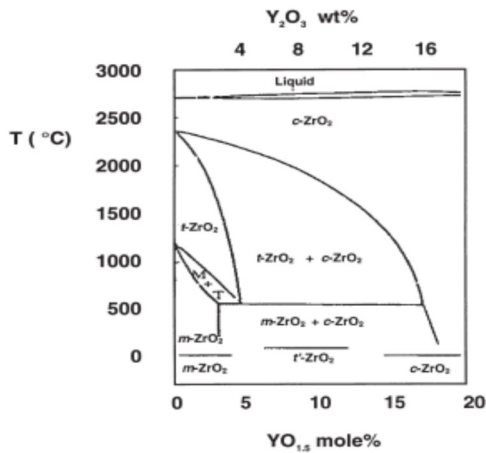

Figure 4. Phase diagram for ZrO_2-Y_2O_3 [30]

The particle morphology and size distribution of zirconia are shown in Figs. 5 a and b. Some of the particles are semi spherical. Small particles are agglomerated together to form aggregates and some

exhausting by the dust collector could be considered. The flowability of this powder was superior to that of the aggregate powder. The morphology of the powders sprayed in water is displayed in Fig. 5 c and d. It is obvious that most of the particles are spheroidized after spraying in water. The average particle size of powders before spraying is 27 μm. After spraying spheroidized powder particle size increases to 50 μm. Fig. 6 shows cross section SEM image of the particles hollow spherical particles (HOSP), fully and semi densified particles. The powder begins to melt when contacted with the spray gun at a high temperature of the plasma jet; also, because of surface energy effect, the particles in molten YSZ powder become spherical. The larger particles created as partially molten of smaller particles after spraying. Some powders when sprayed in water, they became denser, approaching spherical in shape, and had smooth surfaces. Some powders had HOSP shape were indeed the easiest to melt compared to the others. This better heating is due to the lower mass of HOSP particles compared to that of other types of particles [2]. The flowability (30 degree) is much better than that of powders before plasma spraying.

TABLE 3. Mole fraction of YSZ phases before and after spraying in water

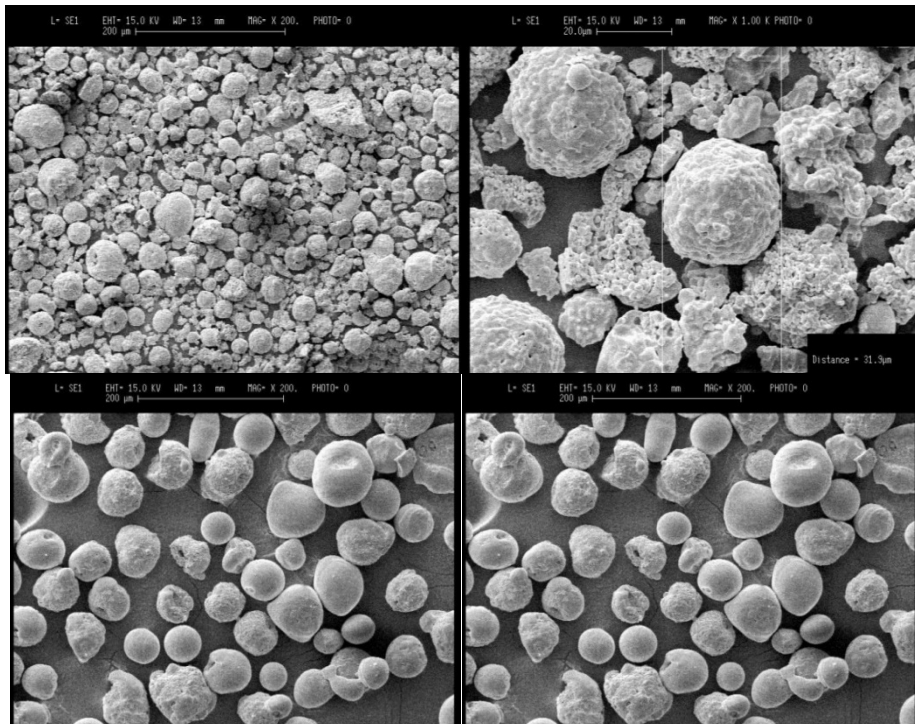|	m		t		c	
	Before spraying	After spraying in water	Before spraying	After spraying in water	Before spraying	After spraying in water
Mole fraction (%)	17	2	33	47	50	51

Figure 5. SEM images of YSZ before spraying in water (a, b) and after spraying in water (c, d)
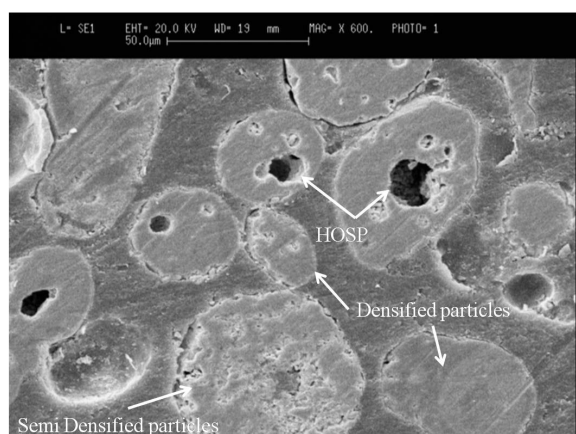
Figure 6. Cross section SEM image of YSZ spherodized powders due to APS procedure

4. CONCLUSIONS

YSZ powders plasma sprayed in water (with parameters mentioned in this research) could be spherodized. All of Phase transformation changes improve the properties of the resulting powders.

The overall results obtained from this research include:

- During the plasma process of Zirconia powder, some monoclinic phases transform to stable tetragonal phase, which improves the properties of the powder.

- Zirconia crystallite size and lattice strain decreased after plasma spraying in water.

- Morphology of Zirconia powder plasma sprayed in water was spherical-like next to a small increase in particle size.

REFERENCES

1. Eslamian, M., Ashgriz, N., "Effect of precursor, ambient pressure, and temperature on the morphology, crystallinity, and decomposition of powders prepared by spray pyrolysis and drying", *Powder Technology,* Vol. 167, (2006), 149-159.

2. Fauchais, P.L., Heberlein, J.V.R. and Boulos, M., Thermal Spray Fundamentals From Powder to Part, Springer Science+Business Media, New York, (2014).

3. Nayebpashaee, N., Aboutalebi, M.R., Seyedein, S., Sarpoolaky, H. and Hadavi, M.M., "Simulation of the effect of sub- micron interface roughness on the stress distribution in functionally graded thermal barrier coatings (FG- TBC)", *Acerp,* Vol. 1, No. 1, 40-47.

4. Zhang, X., Zhou, K., Chang, F., Song, C., Deng, C. and Liangc, S., "Yttria-stabilized-zirconia hollow spheres prepared by atmospheric plasma spray", *Particuology,* Vol. 14, (2014), 57–62.

5. Mobasherpour, I., Salahi, E., Razavi, M. and Asjodi, A., "In vitro evaluation of apatite/wollastonite glass–ceramic nano biocoatings on 316 alloys by plasma-sprayed", Acerp, Vol. 1, No. 3, (2015), 34-38.

6. Padmanabhan, P.V.A., Ramanathan, S., Sreekumar, K.P. and Satpute, R.U., "Synthesis of thermal spray grade yttrium oxide powder and its application for plasma spray deposition", *Materials Chemistry and Physics,* Vol. 106, (2007), 416-421.

7. Girolamo, G.D., Brentari, A. and Serra, E., "Morphology and Microstructure of NiCoCrAlYRe Coatings after Thermal Aging and Growth of an Al2O3-Rich Oxide Scale", *Coatings,* Vol. 4, (2014), 701-714.

8. Ananthapadmanabhan, P.V., Sreekumar, K.P., Venkatramani, N., Kameswaran, R., Dias, C.C. and Mishra, S.C., "Particle morphology and size distribution of plasma processed aluminium powder", *Bulletin of Materials Science*, Vol. 19, (1996), 559-564.

9. Pakseresht, A.H., Rahimipour, M.R., Vaezi, M.R. and Salehi, M., "Effect of splat morphology on microstructure and dielectric property of plasma sprayed Barium titanate films", *Applied Surface Science,* Vol. 324, (2015), 797–806.

10. Pakseresht, A.H., Rahimipour, M.R., Vaezi, M.R. and Salehi, M., "Thermal plasma spheroidization and spray deposition of barium titanate powder and characterization of the plasma sprayable powder", *Materials Chemistry and Physics,* Vol. 173, (2016), 395-403

11. Clarke, D.R. and Levi, C.G., "Materials design for the next generation thermal barrier coatings", *Annual Review of Materials Research,* Vol. 33, (2003), 383–417.

12. Pakseresht, A.H., Rahimipour, M.R., Vaezi, M.R. and Salehi, M., "Effect of morphology and nonbounded interface on dielectric properties of plasma sprayed $BaTiO_3$ Coating", *Journal of Advanced Materials and Processing,* Vol. 2, No. 4, (2014), 25-32.

13. Meier, S.M., Gupta, D.K. and Sheffler, K.D., "Ceramic thermal barrier coatings for commercial gas turbine engines", JOM, Vol. 43, (1991), 50–53.

14. Khan, A.S. and Nazmy, M., "MCrAlY bond coating and method of depositing said MCrAlY bond coating", *United States Patent,* Vol. 531, No 7, (2007).

15. Haynes, J.A., Ferber, M.K. and Porter, W.D., "Thermal Cycling Behavior of Plasma-Sprayed Thermal Barrier Coatings with Various MCrAlX Bond Coats", *Journal of Thermal Spray Technology,* Vol. 9, (2000), 38-48.

16. Song, P., Naumenko, D., Vassen, R., Singheiser, L. and Quadakkers, W.J., "Effect of oxygen content in NiCoCrAlY bondcoat on the lifetimes of EB-PVD and APS thermal barrier coatings", *Surface & Coatings Technology,* Vol. 221, (2013), 207–213.

17. Taylor, M.P., "An oxidation study of an MCrAlY overlay coating", *Materials at High Temperatures Journal,* Vol. 22, (2005), 433–436.

18. Pakseresht, A.H., Rahimipour, M.R., Alizadeh, M., Hadavi, S.M.M. and Shahbazkhan, A., "Concept of Advanced Thermal Barrier Functional Coatings in High Temperature Engineering Components", *Research Perspectives on Functional Micro- and Nanoscale Coatings,* Vol. 396, (2016), 24.

19. Di Girolamo, G., Alfano, M., Pagnotta, L., Taurino, A., Zekonyte, J. and Wood, R.J.K., "On the early stage isothermal oxidation of APS CoNiCrAlY coatings", *Journal of Materials Engineering and Performance*, Vol. 21, (2012), 1989–1997.

20. Williamson, G.K., Hall, W.H., "X-ray Line Broadening from Filed Aluminium and Wolfram", Acta Metallurgica, Vol. 1, (1953) 22–31.

21. Meyers, M.A., Mishra, A., Benson, D.J., "Mechanical properties of nanocrystalline materials", Progress in Materials Science, Vol. 51, (2006), 427–556.

22. Pourghahramani, P. and Akhgar, B.N., "Characterization of structural changes of mechanically activated natural pyrite using XRD line profile analysis", *International Journal of Mineral Processing,* Vol. 134, (2015), 23–28.

23. McPHERSON, R., " A review of microstructure and properties of plasma sprayed ceramic coatings", *Surface and Coatings Technology,* Vol. 39//40, (1989), 173- 181.

24. Toraya, H., Yoshimura, M. and Somiya, S., "Calibration curve for quantitative analysis of the monoclinic-tetragonal ZrO_2 system by X-ray diffraction", Journal of the American Ceramic Society, Vol. 67, (1984), Cl19-C121.

25. Noma, T., Yoshimura, M., Somiya, S., Kato, M., Shibata, M. and Seto, H., "Stability of diffusionlessly transformed tetragonal phases in rapidly quenched ZrO_2-Y_2O_3", *Advances in Ceramics,* Vol. 24, (1988), 377-384.

26. Yashima, M., Ishizawa, N., Noma, T. and Yoshimura, M., "Stable and metastable phase relationships in the system ZrO_2-$ErO_{2.5}$", *Journal of the American Ceramic Society,* Vol. 74, No. 3, (1991), 510-513.

27. Yashima, M., Ishizawa, N., Noma, T. and Yoshimura, M., "Phase transformation temperatures of rare-earths-doped zirconia prepared by arc melting", *Journal of the Ceramic Society of Japan,* Vol. 101, No. 8, (1993), 871-876.

28. Iwamoto, N., Umesaki, N. and Endo, S., " Characterization of plasma-sprayed zirconia coatings by X-ray diffraction and Raman spectroscopy", *Thin Solid Films,* Vol. 127, (1985), 129-137.

29. Díaz, P.A., "Microstructural characterization of a plasma sprayed ZrO_2-Y_2O_3-TiO_2 thermal barrier coating", Brunel University, Uxbridge, United Kingdom (1996).

30. Scott, H.G., "Phase relationships in zirconia-yttria system", *Journal of Materials Science,* Vol. 10, (1975), 1527–1535.